Distortion effects in soft-x-ray energy spectra for xenon gaseous detectors: A Monte Carlo simulation study

T. H. V. T. Dias and F. P. Santos
Departamento de Física, Universidade de Coimbra, 3000 Coimbra, Portugal

A. D. Stauffer
Physics Department, York University, Toronto, Canada M3J IP3

C. A. N. Conde
Departamento de Física, Universidade de Coimbra, 3000 Coimbra, Portugal
(Received 28 January 1992)

Distortion effects observed in soft-x-ray spectra in the 0.1–5-keV range obtained with xenon gaseous detectors are investigated using a detailed Monte Carlo simulation of the absorption of low-energy x-ray photons in xenon at $p=760$ Torr and $T=293$ K, for uniform applied electric fields 100, 500, 1000, 1500, 2000, and 2500 V/cm. Distortion effects are shown to correspond to a loss of electrons to the xenon-filled detector's window, and the influence of the field strength applied in the detector's x-ray-absorption zone is assessed.

PACS number(s): 32.80.−t, 29.40.Cs, 34.90.+q, 07.85.+n

I. INTRODUCTION

A detailed simulation model of the absorption of low-energy x rays in xenon has been developed by the authors, and a full description, including the atomic transition probabilities and scattering cross sections used, is planned to be published separately [1]. In the present paper we present results of a study of the distortion effects in the soft-x-ray spectra obtained in gaseous detectors by using this model. The model includes all atomic processes that produce electrons, from the initial photoionization of the xenon atom to the subsequent cascade processes due to inner shell vacancies involving Auger–Coster-Kronig transitions, fluorescence emission, and electron shakeoff [2–4], and the subsequent ionization of the xenon atoms by energetic electrons. This sequence of atomic processes produces numerous electrons with various energies for each initial x-ray–atom interaction.

We have previously used this model to study xenon-filled gas proportional scintillation counters (GPSC) with an externally applied low electric field typical of that used in the drift region of these detectors. The simulation followed the histories of the electrons produced in the gas which involved multiple elastic and inelastic (both excitation and ionization) collisions with the neutral xenon atoms until the primary electron cloud was fully grown, i.e., until the kinetic energy of every electron produced fell below the first ionization potential of xenon. This previous work has produced some quite interesting results. We have found that the computed Fano factor [5] and w values (the mean energy to produce an electron-ion pair in the absorbing media) [6] proved to depend significantly on the energy of the incident x ray. These effects, together with intrinsic energy linearity variations [6] have been experimentally observed [7], but their cause was not well understood until now. We have also investigated the size of the primary electron cloud [8], an aspect which is of interest for imaging detectors.

In our previous studies referred to above, no real physical boundaries were introduced in the simulation, so that the computed energy spectra—given in terms of a frequency plot of the number N of primary (i.e., subionization) electrons produced by incident photons of a given energy—did not reflect effects like the loss of primary, or higher-energy, electrons to the detector window.

The experimental work of Inoue *et al.* [9] and Hamilton *et al.* [10] with xenon-filled GPSC's, using x-ray energy sources below 2 keV, has shown a clear tail enhancement of the spectra obtained, which was explained in terms of the diffusion of the primary electron cloud to the x-ray entrance window [9] due to the small penetration depths involved. X-ray penetration depths can indeed become very small for soft x rays, particularly when their energies lie just above the first xenon absorption edges [$N_{4,5}$(68.5 eV) and $M_{4,5}$(683 eV), for instance] where the photoionization cross sections exhibit large peaks, as shown in Fig. 1.

To overcome the degradation of the low-energy response of conventional GPSC's (i.e., GPSC's with two separate regions, the drift and the scintillation regions), Simons and de Korte [11,12] designed a driftless, xenon-filled, parallel plate GPSC for the energy range 0.1–25 keV, where electron loss to the window for soft x rays is reduced since a strong electric field is established near the window. A burst length (scintillation pulse length) correction was introduced above 2 keV to overcome the resolution degradation caused by the x-ray photons being absorbed directly in the scintillation region at various depths.

In the present work we will simulate the absorption of low-energy x rays in xenon and calculate the corresponding energy spectra produced under different uniform ap-

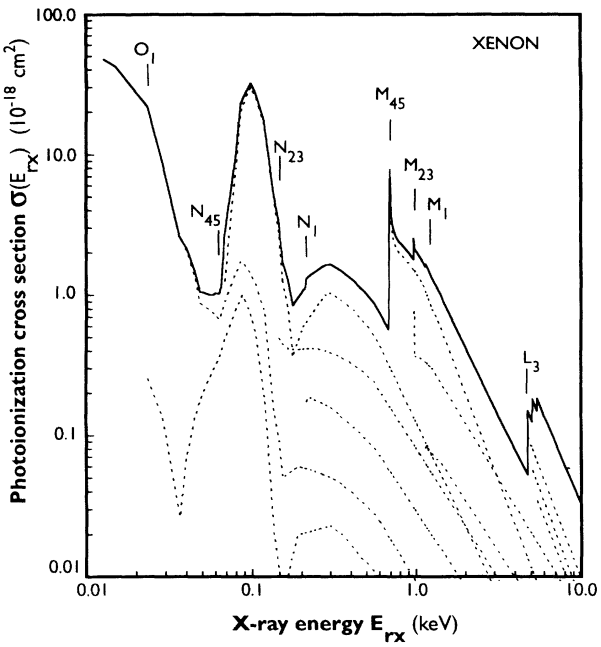

FIG. 1. Total (——) and partial (— — —) xenon photoionization cross sections for soft x rays [1].

plied electric fields when the electrons are allowed to be captured by a hypothetical x-ray entrance window. The calculated results will show that this electron loss can indeed account for the distortion effects which have been observed experimentally. Preliminary results obtained for x rays near the $M_{4,5}$ absorption edge were previously reported for two electric fields [13].

The approach described here will apply not only to GPSC's but also to standard (ionization) proportional counters and to ionization chambers.

II. THE SIMULATION METHOD

In order to obtain the x-ray energy spectra when the possibility of losing electrons back to the window is taken into account (with the window located at $Z=0$, and $Z>0$ the distance from the window measured inside the gas), the Monte Carlo method was used to simulate the histories of all electrons produced during vacancy cascade decay and electron impact ionization of the xenon atoms. These histories are terminated when the electron hits the window ($Z\leq 0$) or when primary electron return becomes energetically excluded. As the electric field is conservative, this no-return condition will be attained when the primary electron's energy $\mathcal{E}$ (eV) is smaller than the field equipotential energy at its current position Z (cm), i.e., when the energy lost in the successive collisions is such that the relation $\Delta=\mathcal{E}-ZE\leq 0$ is satisfied, where E (V/cm) is the applied electric field (assumed to be uniform).

For a given x-ray energy, this is in general a much more computer-intensive problem than that of the simulation of the growth of the primary electron cloud [5,6,8]: in fact, depending on the strength of the electric field considered, the number of primary electrons with $\Delta>0$ may be very large and each one of them may have to undergo a huge number of elastic collisions with xenon atoms (electrons lose only a very small fraction of their energy in these collisions) before its fate gets decided by either Z or Δ becoming negative.

For this reason, in order to avoid following each electron produced after an x-ray photon absorption all the way down to the final "hit/miss" decision, preliminary simulations were performed for each electric field to obtain a reasonable set of values for the probability $P(\mathcal{E}_s,Z_k)$ that a subexcitation electron at a position Z_k with energy $\mathcal{E}_s$ and $\Delta>0$ will end up hitting the window (i.e., will ever reach $Z\leq 0$). This was achieved by "injecting" directly into the simulation program a sample of N subexcitation electrons, considering various energies $\mathcal{E}_s<8$ eV (a limit which guarantees only elastic collisions take place, as xenon excitation and ionization thresholds equal 8.32 and 12.1 eV, respectively) and various starting positions $Z_k<D=\mathcal{E}_s/E$ [for $Z\geq D$, $P(\mathcal{E}_s,Z_k)$ is necessarily zero, as Δ is then negative]. N electrons are followed until their histories end. Each P value is just the relation between the obtained number of "hits" to the number N of "injected" electrons. To compute each $P(\mathcal{E}_s,Z_k)$ value, $N=2500$ electrons were considered with each initial direction taken from an isotropic distribution. A mesh of points was chosen with a step in $\mathcal{E}_s$ of 0.1 eV up to 4 eV, 0.5 eV from 4 to 8 eV, and a 1-μm step in Z_k. Figure 2 represents the $P(\mathcal{E}_s,Z_k)$ surface obtained for $E=100$ V/cm.

Particularly for the lowest electric fields, the speed of the simulation dealing with the absorption of any x rays, which ultimately yields the x-ray spectra we wanted to obtain, was greatly increased by the use of these $P(\mathcal{E}_s,Z_k)$ surfaces: the history of each electron produced after x-ray absorption is followed directly (i.e., collision

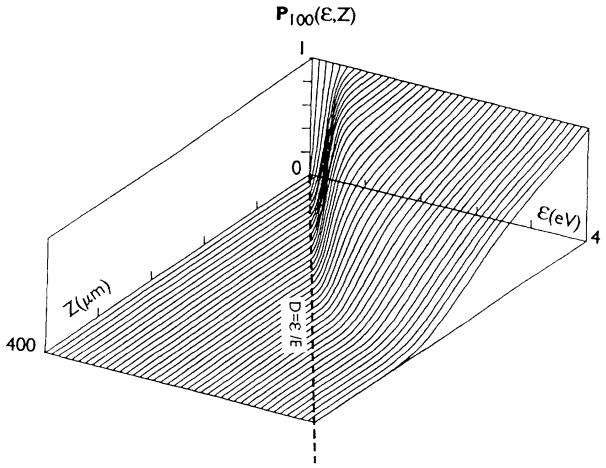

FIG. 2. For an applied electric field of 100 V/cm, $P_{100}(\mathcal{E},Z)$ represents the computed probability that an electron produced after the absorption of x-ray photons in Xe at atmospheric pressure and reaching an energy $\mathcal{E}<8$ eV will eventually, in the course of its later history, hit the detector's window. Probability curves are represented at 0.1 eV steps from $\mathcal{E}=0.1$ to 4.0 eV.

after collision) only while their energy stays larger than 8 eV, as below this energy their fate (hit or miss the window) is then immediately decided by comparing a random number from a uniform distribution in (0,1) with the value $P(\mathcal{E},Z)$ obtained through interpolation over the $P(\mathcal{E}_s,Z_k)$ surface for the current electric field.

Let us now look with more detail into the way the points on the probability surfaces were calculated. To compute each sequence of probabilities $P(\mathcal{E}_s,Z_1),P(\mathcal{E}_s,Z_2),P(\mathcal{E}_s,Z_3),\ldots,P(\mathcal{E}_s,D)$, in principle the sample of N electrons with energy $\mathcal{E}_s$ would be successively injected at the points Z_1, Z_2, Z_3, etc. and followed in the simulation, yielding, for each Z_k, a number H_k of "hits" and M_k of "misses" ($M_k+H_k=N$) and giving $P(\mathcal{E}_s,Z_k)=H_k/N$. However, this sequence of simulations does not have to be initialized anew with N electrons at every Z_k in the series (actually this proved to require an excessive amount of computer time in some cases): equivalent results were actually obtained with an ever-decreasing sample of electrons ($n_1=N>n_2>n_3$ etc.) with the sequence of calculations obeying $Z_1<Z_2<Z_3$ etc. In fact, after obtaining $P(\mathcal{E}_s,Z_1)$ by injecting the sample of N electrons at Z_1 and obtaining H_1 "hits" (H_1 electrons lost to the window, with current path for electron i "ending" outside the window at $Z=Zh_1^i\le 0$) and M_1 "misses" ($M_1+H_1=N$), it is a waste of computing time to follow again the whole sample from Z_2 in order to obtain $P(\mathcal{E}_s,Z_2)$: part of this simulation has already bee done during the first stage (electrons starting from point Z_1) apart from a shift of Z_2-Z_1 in the electron distances to the window. This means that starting with N electrons injected at Z_2 is equivalent to take for sure M_1 "misses" (notice that this is only true if $Z_2>Z_1$) and follow only $n_2=H_1$ electrons (the previous number of "hits"), as far as we "pull" back each one of these electrons to a starting position $Z_2^i=Z_2-(Z_1+|Zh_1^i|)$, with the energies $\mathcal{E}^i$ and the directions they had at $Zh_1^i<0$. This second stage simulation will result in a number H_2 of "hits" and a number m_2 of "misses" ($m_2+H_2=n_1$), giving $P(\mathcal{E}_s,Z_2)=H_2/N$. In general, for the stage starting at Z_k, it is sufficient to initiate the simulation with only $n_k=H_{k-1}$ electrons, assuming M_{k-1} "misses" for sure, and locating electron i ($1\le i\le n_k$) at a starting position $Z_k^i=Z_k-(Z_{k-1}+|Zh_{k-1}^i|)$ (instead of the common point Z_k), with the energies and directions from the preceding stage "hit window" positions Zh_{k-1}^i. The sequence will end when $H_k=0$. We summarize the $P(\mathcal{E}_s,Z_k)$ series computation scheme ($k=1,2,\ldots,f$) in Fig. 3 and as follows:

$n_1=N$	$n_1=M_1+H_1$		$P(\mathcal{E}_s,Z_1)=H_1/N$
$n_2=H_1$	$n_2=m_2+H_2$	(i.e., $N=[M_1+m_2]+H_2=M_2+H_2$)	$P(\mathcal{E}_s,Z_2)=H_s/N$
$n_3=H_2$	$n_3=m_3+H_3$	(i.e., $N=[M_2+m_3]+H_3=M_3+H_3$)	$P(\mathcal{E}_s,Z_3)=H_3/N$
. . .	. . .	. . .	. . .
$n_k=H_{k-1}$	$n_k=m_k+H_k$	(i.e., $N=[M_{k-1}+m_k]+H_k=M_k+H_k$)	$P(\mathcal{E}_s,Z_k)=H_k/N$
. . .	. . .	. . .	. . .
$n_f=H_{f-1}$	$n_f=m_f+0$	(i.e., $N=[M_{f-1}+m_f]+0=M_f+0$)	$P(\mathcal{E}_s,Z_f)=0/N$

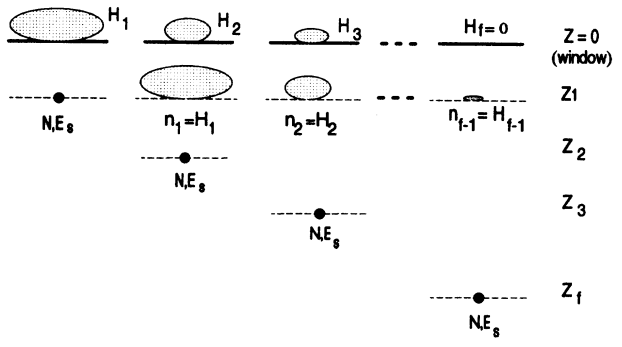

FIG. 3. Computation scheme used to obtain, for a given electron energy $\mathcal{E}_s<8$ eV, the sequence of probability values $P(\mathcal{E}_s,Z_k)$, $k=1,2,3,\ldots,f$. As $Z_k-Z_{k-1}=Z_1$ ($Z_1=1$ μm) was adopted, any stage k, which represents N electrons with $\mathcal{E}_s$ starting at Z_k, starts instead with $n_k<n_{k-1}<N$ electrons with energies $\mathcal{E}^i<\mathcal{E}_s$ at positions $Z_k^i<Z_1$ (see text).

In terms of computing time, simulating one $\mathcal{E}_s$ series this way is equivalent to following the sample of N electrons from one starting position only: the distance Z_f. All the previous stages can actually be seen as partial simulations of this fth stage. This scheme proved to have the additional advantage of finding, without any computing time effort, where the "every electron misses" frontier Z_f is located, which, for a large enough value of $\mathcal{E}_s$, happens to be smaller than the obvious first choice $D=\mathcal{E}_s/E$, as can be seen in Fig. 2.

III. RESULTS AND DISCUSSION

Twenty-five x-ray energy spectra were computed for the absorption of x rays with energies between 68 and 4785 eV for six applied electric fields: 100, 500, 1000, 2000, and 2500 V/cm. The absorption of 25 000 photons was considered in each case. For each x-ray energy, the six spectra are compared with what we call the reference spectrum for that energy, which is the spectrum obtained when no frontier window was considered [5,6]. As can be seen along the calculated energy spectra represented in

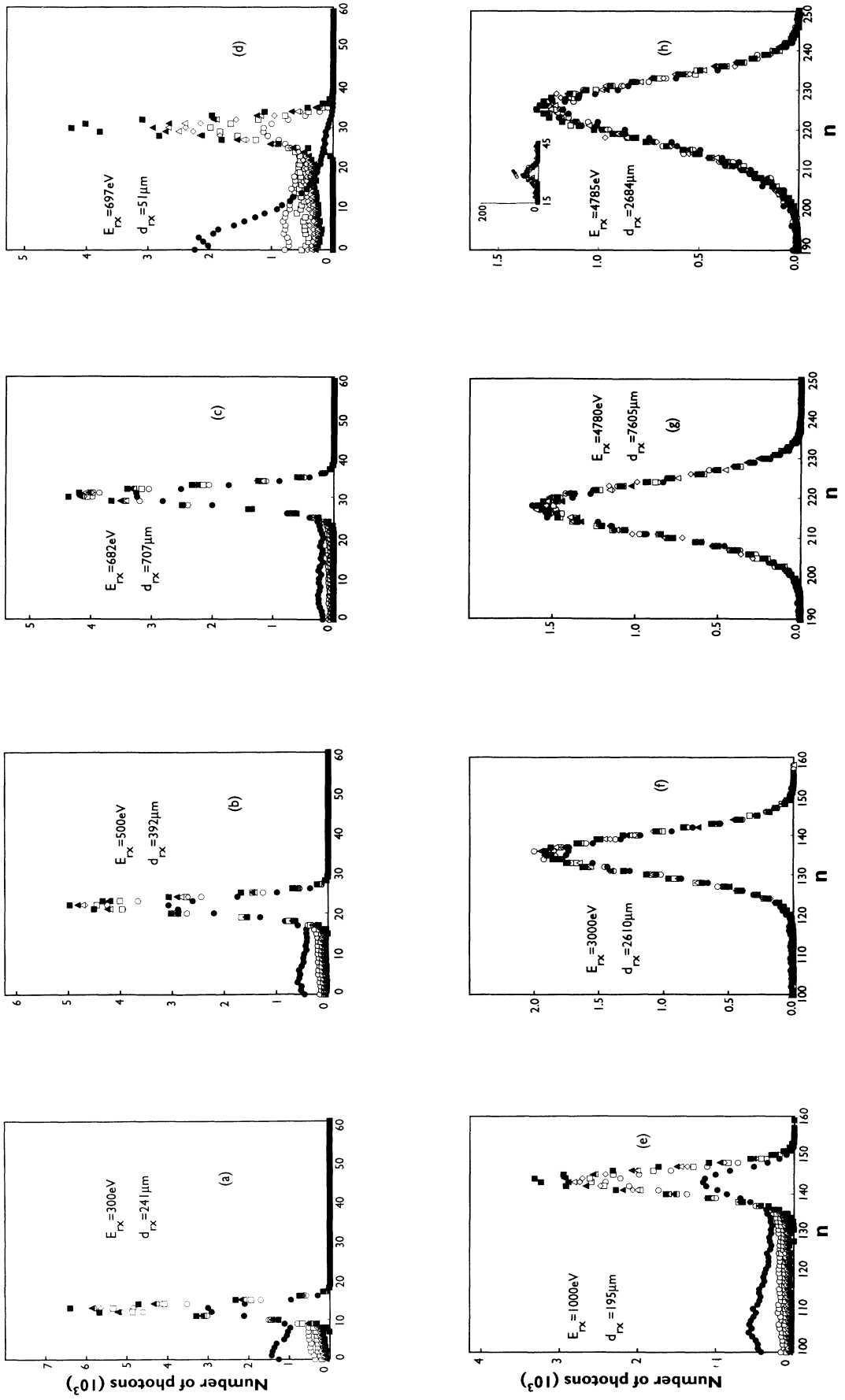

FIG. 4. Computed x-ray energy spectra (number of absorbed photons vs number n of primary electrons produced per photon) in Xe at 760 Torr, 293 K, for eight different x-ray energies [(a)–(h)] and for six different applied electric fields: 100 V/cm (●), 500 V/cm (○), 1000 V/cm (□), 1500 V/cm (◇), 2000 V/cm (△), and 2500 V/cm (▲). For each energy, the reference spectrum (■) is represented, corresponding to the case where electron loss to the window was neglected. All spectra represented were calculated with 25 000 absorbed x-ray photons.

Figs. 4(a)–4(h) (eight examples taken from the sequence of 25 x-ray energies treated in this work), a significant tail enhancement may occur, where the distortion can go as far as a complete dislocation towards the low end side of the spectra. For each x-ray energy, the largest effect occurs for the lowest electric field (●, $E=100$ V/cm), and in general the effect will decrease as the field is increased, with the spectra gradually approaching the reference spectrum (■), except for the case of 98 eV (not depicted in Fig. 4) where a peak could never be seen.

Figures 4(a)–4(h) clearly show that a correlation exists between the distortion of the spectra and the value of the average x-ray penetration depth d_{rx}, showing that in general the tail diminishes as d_{rx} increases, with the worst case corresponding to the shortest d_{rx} value for the x-ray energies E_{rx} represented in Fig. 4 (51 μm at $E_{rx}=697$ eV). The absorption lengths were calculated as $d_{rx}=1/[\sigma(E_{rx})n]$, with $\sigma(E_{rx})$ the value, at E_{rx}, of the photoionization cross section used in the simulation (Fig. 1), and n the number density (at 760 Torr and 293 K, the conditions used in this work).

The tail enhancement effect can be most visible for x-ray energies near those atomic absorption edges where the photoionization cross section $\sigma(E_{rx})$ exhibits maxima and d_{rx} minima. For instance, the 697-eV(M_{45}^{+}) x-ray spectra [Fig. 4(d)] [an energy matching the maxima in $\sigma(E_{rx})$ *above* the M_{45} absorption edge, see Fig. 1] correspond to the shortest d_{rx} value (51 μm) and show important deviations at any of the electric fields used: as electrons are produced very near the detector's window, a significant fraction can be lost back to the entrance. However, the spectra of 682-eV (M_{45}^{-}) x rays [Fig. 4(c)] (an energy matching the minima *below* the same edge) appear much less distorted, as the corresponding d_{rx} is much longer (707 μm). Near the L_3(4782.2 eV) threshold [Figs. 4(g) and 4(h)] the effect is not so important: although it is true that $d_{rx}(L_3^{+})\ll d_{rx}(L_3^{-})$, the fact is that $d_{rx}(L_3^{+})$ is nevertheless very large, and electrons are in general produced deep within the gas.

In order to analyze quantitatively the deterioration of the energy spectra from the point of view of electron loss to the window, we list in Table I, for each one of the 25 x-ray energies considered, and as a function of the applied electric field, the percentage a of primary electrons counted within each calculated spectrum and the percentage b of primary electrons captured by the window, referred to the total number of primary electrons produced when spatial restrictions are not introduced (reference spectrum). We can see that the electron losses reach the highest peaks at the energies labeled N_{45}^{+} and M_{45}^{+}, where the primary electrons escape at $E=100$ V/cm reaches 91% and 72%, respectively. The efficiency with which primary electrons are collected is very sensitive to the field, but observing Table I we can conclude that important losses (say over 10%) cannot in general be avoided for x rays with energies below ~ 1.5 keV for electric fields lower than 760 V/cm (i.e., $E/p=1$ V cm^{-1} Torr^{-1}), a fact that is important in GPSC's with a drift region, where a reduced electric field lower than the scintillation threshold ($E/p=1$ V cm^{-1} Torr^{-1} in xenon) must be used.

For each x-ray energy, the sum of the quantities a and b in Table I amounts in general to less than 100%, and remains approximately constant along the range of applied electric fields used in this work. The difference from 100% [$\sim 2\%$ at 98 eV(N_{45}^{+}), $\sim 3\%$ at 697 eV(M_{45}^{+}), $\sim 2\%$ at 4785 eV(L_3^{+}), and lower at all other energies listed], is related to the loss of high-energy, nonprimary electrons (Auger electrons, for instance) which are not much influenced by the field, and with the escape of x-ray fluorescence photons through the window, obviously insensitive to the field. X-ray fluorescence emission is only important for energies above the L_3 threshold, and for the energy 4785 eV (L_3^{+}) its escape is enough to account for the mentioned field independent losses, causing the appearance in its six spectra of a distinct small peak centered at ~ 30 electrons, as shown in Fig. 4(h), upper left corner.

In Fig. 5 we plot, as a function of the applied electric field, the percentage Q of the area of each calculated x-ray energy spectrum which falls above and to the left of the corresponding reference spectrum, a quantity which can be seen as a distortion indicator, where each spec-

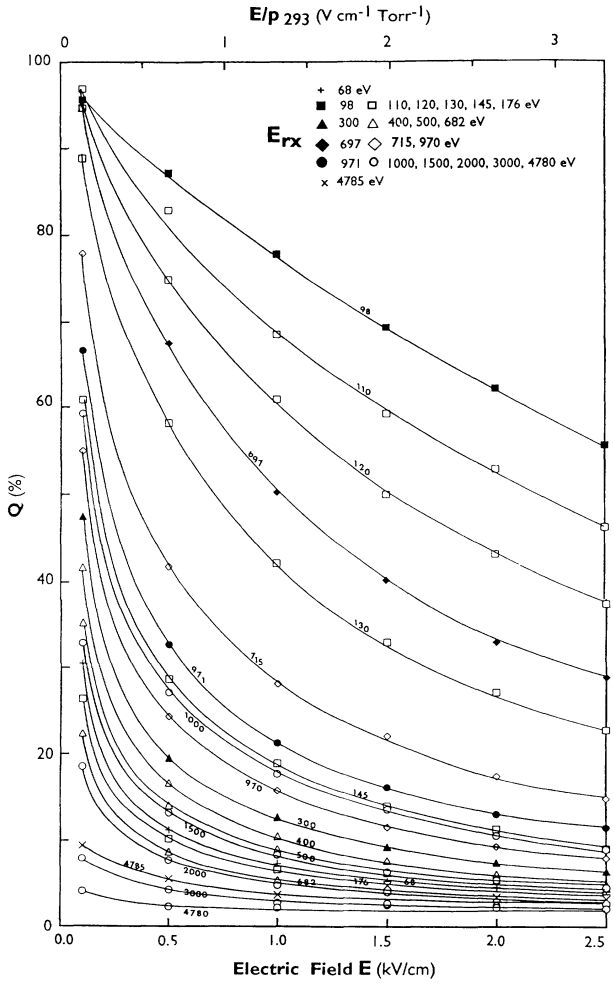

FIG. 5. Percentage Q of the area of each calculated x-ray spectrum which falls above and to the left of the corresponding reference spectrum, as a function of the applied electric field E.

trum always corresponds to a total area of $N=25\,000$ photons as stated above. Q is calculated as

$$Q(\%)=100\sum_{j=1}^{l}[s(j)-r(j)]/N\ ,$$

where $s(j)$ and $r(j)$ are the number of photons in channel j in the current spectrum and in the reference spectrum, respectively, and l is the channel where the two spectra intersect. For each x-ray energy, the improvement observed with the increasing electric field applied is clear,

TABLE I. Percentage of primary electrons (*a*) counted and (*b*) captured by the window as a function of the applied electric field E, for different x-ray energies E_{rx} and penetration lengths d_{rx} (Xe 760 Torr, 293 K).

			E (V/cm)				
E_{rx} (eV)	d_{rx} (μm)	100	500	1000	1500	2000	2500
68(N_{45}^{-})	295	(*a*) 71.6%	89.6	93.0	95.3	96.0	96.0
		(*b*) 28.4%	10.4	6.7	4.7	3.9	3.9
80	39	18.3	47.2	61.7	69.9	75.3	79.9
		81.0	52.3	37.9	29.5	24.3	20.1
98(N_{45}^{+})	13	7.1	20.6	31.7	40.0	46.9	53.1
		91.1	77.5	66.7	58.3	51.2	45.0
110	17	9.5	27.1	40.2	49.3	56.1	62.1
		88.8	71.2	58.3	49.1	42.3	36.5
120	25	13.0	36.6	50.8	60.2	66.5	71.0
		85.9	62.3	47.8	38.7	32.3	27.8
130	45	22.0	52.8	66.5	74.0	78.7	82.1
		77.5	46.6	32.9	25.5	20.5	17.2
145	134	50.7	78.6	86.0	90.0	91.9	93.5
		49.0	21.1	13.7	9.9	7.8	6.3
176	469	80.3	92.9	95.3	96.9	97.7	98.0
		19.7	6.9	4.5	2.9	2.3	1.9
225	290	71.0	88.8	93.6	94.9	96.4	96.7
		28.9	10.9	6.2	4.7	3.6	3.1
300	241	66.8	87.2	92.0	94.3	95.5	96.3
		32.8	12.4	7.8	5.5	4.3	3.5
400	304	71.7	89.6	93.6	95.3	96.4	97.2
		27.8	10.0	6.1	4.4	3.4	2.6
500	392	77.1	91.5	94.9	96.3	96.9	97.6
		22.4	7.9	4.6	3.2	2.6	2.0
682(M_{45}^{-})	707	86.4	95.2	97.1	97.9	98.3	98.7
		13.2	4.4	2.5	1.8	1.4	1.0
697(M_{45}^{+})	51	25.1	56.5	69.9	76.4	81.0	83.5
		71.8	40.1	26.8	20.2	15.6	13.0
715	112	45.5	75.0	83.5	87.6	90.2	91.6
		52.9	23.3	14.7	10.6	8.0	6.6
800	170	50.4	82.3	88.8	91.7	93.5	94.6
		41.7	16.7	10.1	7.2	5.5	4.4
970(M_{23}^{-})	225	65.1	86.3	91.3	93.7	95.0	95.8
		34.0	12.8	7.8	5.4	4.1	3.4
971(M_{23}^{+})	159	55.9	81.2	88.4	91.3	93.1	93.9
		42.9	17.5	10.6	7.6	5.7	4.9
1000	195	61.3	84.3	90.1	92.5	94.3	95.3
		37.8	14.7	8.9	6.5	4.7	3.8
1250	301	71.8	89.4	93.5	95.1	96.2	97.0
		27.5	9.9	5.8	4.1	3.1	2.4
1500	465	80.5	93.0	95.7	96.8	97.2	97.8
		18.9	6.3	3.6	2.5	2.1	1.5
2000	970	89.6	96.4	97.7	98.3	98.7	98.9
		9.9	3.0	1.8	1.2	0.8	0.6
3000	2610	95.9	98.6	99.1	99.2	99.4	99.3
		3.8	1.0	0.5	0.3	0.2	0.2
4780(L_3^{-})	7605	98.5	99.5	99.5	99.7	99.7	99.7
		1.2	0.3	0.2	0.1	0.1	0.1
4785(L_3^{+})	2684	94.9	97.3	97.8	97.8	98.2	98.1
		3.1	0.9	0.4	0.3	0.2	0.2

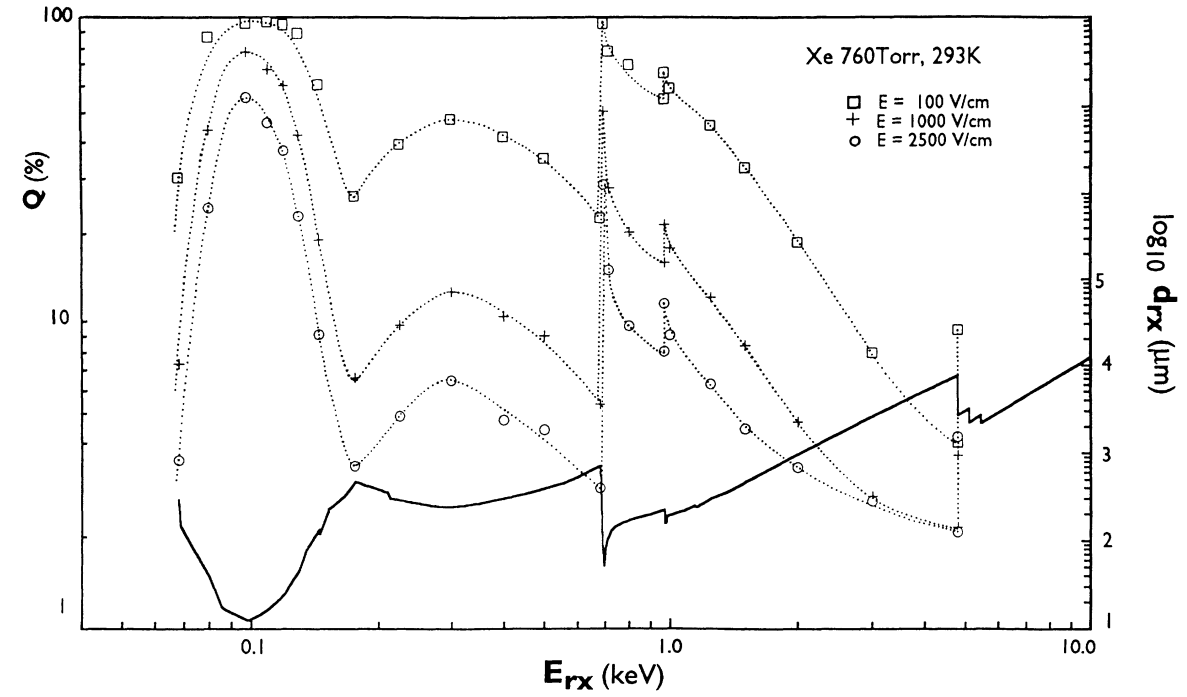

FIG. 6. $Q(\cdots)$, same as in Fig. 5, and absorption length d_{rx} (——) as a function of x-ray energy, for the applied electric fields $E = 100$, 1000, and 2500 V/cm.

showing in each case the progressive ability of the field to bend the electrons' trajectories away from the entrance window. The lower curves belong to the deeper penetration depths, when most primary electrons are already produced deep in the gas, leading to very small losses and low slope of the curves. From Fig. 5 we can verify that, for the same applied electric field, Q is far from being monotonic with x-ray energy as it is bound to reflect the peculiarities of the photoionization cross section $\sigma(E_{rx})$ and of the x-ray path length $d_{rx}(E_{rx})$ as already ex-

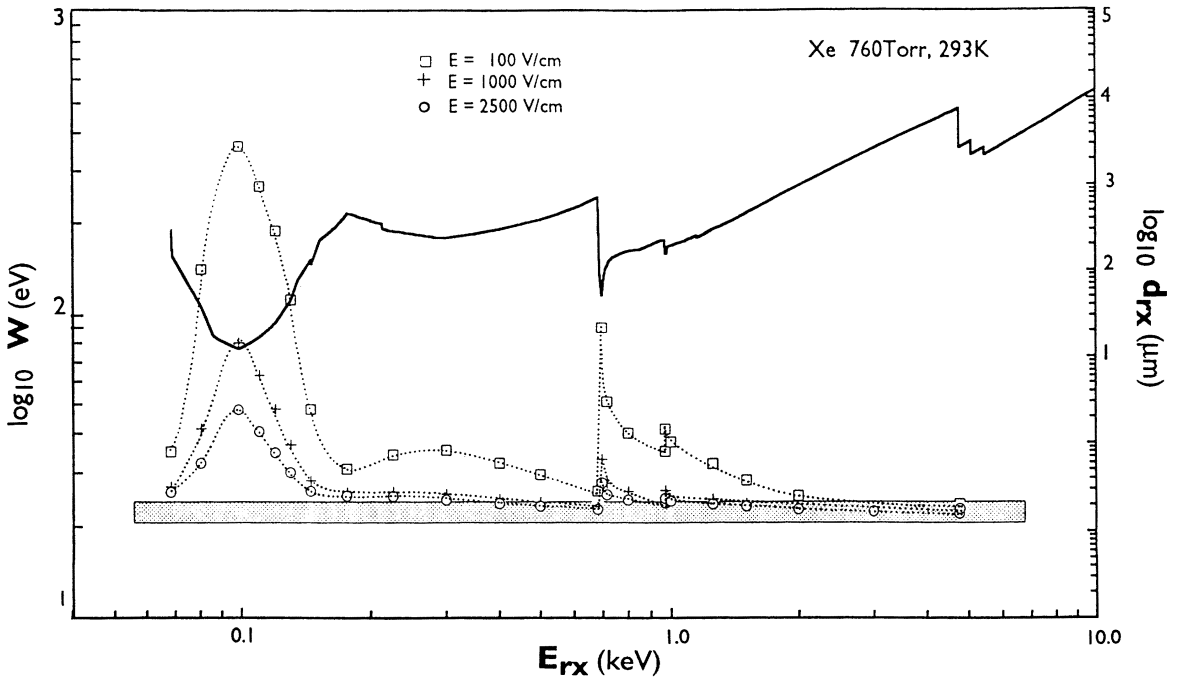

FIG. 7. Calculated effective mean energy per ion pair $w(\cdots)$, and absorption length d_{rx} (——) as a function of x-ray energy, for the applied electric fields $E = 100$, 1000, and 2500 V/cm. Intrinsic w values [6] fall within the gray band.

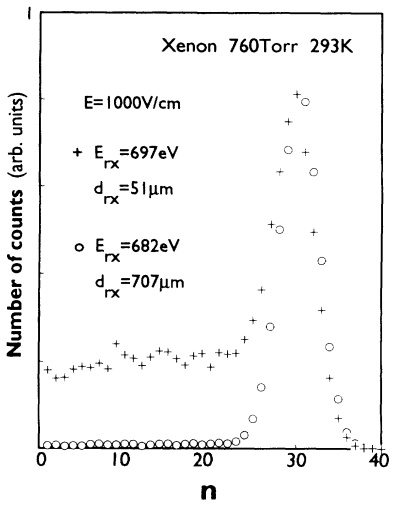

FIG. 8. 682 eV/(M_{45}^-) and 697 eV(M_{45}^+) computed x-ray energy spectra at $E=1000$ V/cm, showing the tail enhancement effect introduced by the M_{45}(683 eV) absorption edge. As in Fig. 4, n represents the number of primary electrons produced per absorbed x-ray photon.

plained. This is shown in Fig. 6, where we represent the parameter Q as a function of the x-ray energy for three electric fields: 100, 1000, and 2500 V/cm.

On the other hand, if we define the effective mean energy per ion pair produced on absorption of x-ray photons, w, as the total energy absorbed in the gas divided by the number of primary electrons counted in the corresponding spectrum, this quantity will also present wide variations with x-ray energy, following again the shape of the varying $\sigma(E_{rx})$ and $d_{rx}(E_{rx})$, as electron losses do. This is shown in Fig. 7, where again the 100-, 1000-, and 2500-V/cm curves are represented. The w variation with energy shown in Fig. 7 is much wider than the theoretical w variation previously obtained when no loss to the window effects was introduced in the simulation [6]. In that case, it was found that, while following the $\sigma(E_{rx})$ trend, w varied within a range of ~ 3 eV only, its values falling within the gray band represented in Fig. 7. This w intrinsic energy dependence was explained in terms of the photon–xenon-atom interaction, whose result does depend on which xenon atomic subshells are photoionized on x-ray absorption.

In Fig. 8 we show, for an applied electric field $E=1000$ V cm^{-1} ($E/p \sim 1.3$ V cm^{-1} Torr^{-1}), the 682(M_{45}^-) and 697 eV(M_{45}^+) pair of spectra computed in this work [as in Figs. 4(c) and 4(d)], now normalized to a common maximum, in order to demonstrate the tail enhancement effect introduced by the M_{45} absorption edge. A close resemblance is found between the spectra in Fig. 8 and the experimental results shown by Inoue *et al.* at $E/p=1$ V cm^{-1} Torr^{-1} (Fig. 2 on p. 296 of [9]) for the pair of x-ray energies 677 eV(F K) and 705 eV(Fe L), also separated by and lying close to the M_{45} threshold. The agreement with these authors is equally successful where we have spectra at similar energies, including the case of our 98- or 110-eV and their 109-eV (Be K) spectra where no peak is visible in the three cases.

IV. CONCLUSIONS

Our Monte Carlo simulation results for absorption of low-energy x rays in gaseous xenon show that important distortions may occur in the energy spectra, a phenomenon which is explained in terms of loss of electrons to the entrance window, and related to the low magnitude of the x-ray-absorption length in the energy range studied. The role played by the applied electric field in lessening this effect is studied for xenon at 760 Torr, 293 K.

The degradation of energy spectra for soft x rays is important in conventional gas proportional scintillation counters, where the upper limits for the electric field that can be applied in the absorption/drift region is $E \sim 760$ V cm^{-1} at atmospheric pressure, if an additional resolution degradation caused by scintillation in that region is to be avoided (the xenon secondary scintillation threshold lies near $E/p \sim 1$ V cm^{-1} Torr^{-1}). Our calculated results, summarized in Fig. 5 and in Table I, explain the tail enhancement and poor resolution effects described in the literature for soft x rays, and are in agreement with what had already been experimentally observed for x-ray spectra below ~ 2 keV in xenon-filled conventional GPSC's [9–12]. Our work shows, however, that, while keeping in mind that sudden changes arise in the magnitude of the effect caused by the loss of electrons through the window when the x-ray energy increases above a new absorption edge, for example, M_{45}, there is still space for improvement in some cases by choosing the highest possible drift field in order to ameliorate the collection of the electrons produced and the consequent spectra in these conventional GPSC's. Let us take two examples from Fig. 5: when we move from $E=100$ to 760 V/cm, at $E_{rx}=300$ eV the parameter Q decreases from 47% to 16% and at $E_{rx}=1500$ eV, Q is lowered from 33% to 10%.

ACKNOWLEDGMENTS

This work was supported by INIC (Instituto Nacional de Investigação Científica), by JNICT (Junta Nacional de Investigação Científica e Tecnológica), and by LNETI (Laboratório Nacional de Engenharia e Tecnologia Industrial) through EUREKA Project No. EU.39.

[1] T. H. V. T. Dias, F. P. Santos, C. A. N. Conde, and A. D. Stauffer (unpublished).
[2] T. Mukoyama, J. Phys. Soc. Jpn. **55**, 3054 (1986).
[3] M. O. Krause and T. A. Carlson, Phys. Rev. **158**, 18 (1967).
[4] T. A. Carlson and C. W. Nestor, Jr., Phys. Rev. A **8**, 2887 (1973).
[5] T. H. V. T. Dias, F. P. Santos, A. D. Stauffer, and C. A. N. Conde, Nucl. Instrum. Methods A **307**, 341 (1991).
[6] F. P. Santos, T. H. V. T. Dias, A. D. Stauffer, and C. A. N.

Conde, Nucl. Instrum. Methods A **307**, 347 (1991).
[7] T. Z. Kowalski, A. Smith, and A. Peacock, Nucl. Instrum. Methods A **279**, 567 (1989).
[8] T. H. V. T. Dias, F. P. Santos, and C. A. N. Conde, Nucl. Instrum. Methods A **310**, 137 (1991).
[9] H. Inoue, K. Koyama, M. Matsuoka, T. Ohashi, and Y. Tanaka, Nucl. Instrum. Methods **157**, 295 (1978).
[10] T. T. Hamilton, C. J. Hailey, W. H.-M. Ku, and R. Novick, IEEE Trans. Nucl. Sci. **NS-27**, 190 (1980).
[11] D. G. Simons, Ph.D. thesis, Leiden University, Holland, 1988.
[12] D. G. Simons and P. A. J. de Korte, Nucl. Instrum. Methods A **277**, 642 (1989).
[13] F. P. Santos, T. H. V. T. Dias, A. D. Stauffer, and C. A. N. Conde, in *Summary Transactions of the 5th International Symposium on Radiation Physics, Dubrovnik, Croatia, Yugoslavia, 1991,* edited by A. Ljubicic (Ruder Boskovic Institute, Zagreb, 1991), p. ii-23.

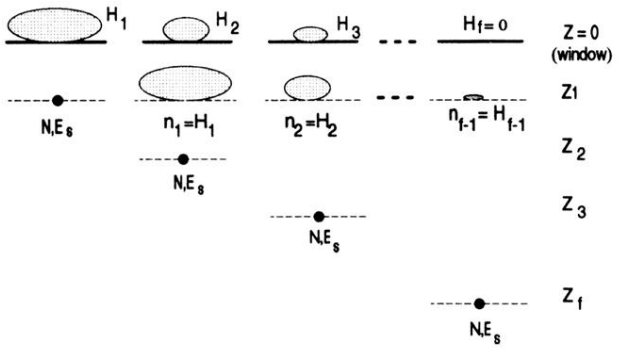

FIG. 3. Computation scheme used to obtain, for a given electron energy $\mathcal{E}_s < 8$ eV, the sequence of probability values $P(\mathcal{E}_s, Z_k)$, $k = 1,2,3,\ldots,f$. As $Z_k - Z_{k-1} = Z_1$ ($Z_1 = 1\ \mu$m) was adopted, any stage k, which represents N electrons with $\mathcal{E}_s$ starting at Z_k, starts instead with $n_k < n_{k-1} < N$ electrons with energies $\mathcal{E}^i < \mathcal{E}_s$ at positions $Z_k^i < Z_1$ (see text).

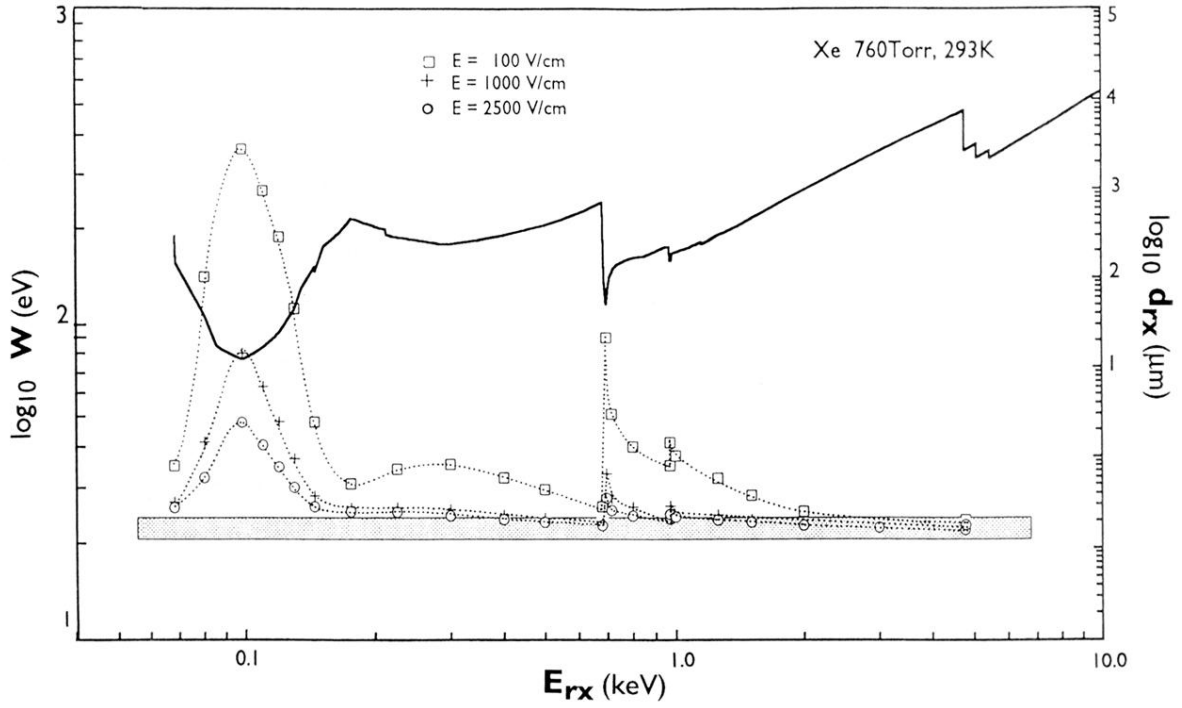

FIG. 7. Calculated effective mean energy per ion pair w($\cdots$), and absorption length d_{rx} (——) as a function of x-ray energy, for the applied electric fields $E = 100$, 1000, and 2500 V/cm. Intrinsic w values [6] fall within the gray band.